High-Fidelity Universal Gate Set for $^9Be^+$ Ion Qubits

J. P. Gaebler, T. R. Tan,* Y. Lin,† Y. Wan, R. Bowler,‡ A. C. Keith, S. Glancy, K. Coakley, E. Knill, D. Leibfried, and D. J. Wineland
National Institute of Standards and Technology, 325 Broadway, Boulder, Colorado 80305, USA
(Received 31 March 2016; published 4 August 2016)

We report high-fidelity laser-beam-induced quantum logic gates on magnetic-field-insensitive qubits comprised of hyperfine states in $^9Be^+$ ions with a memory coherence time of more than 1 s. We demonstrate single-qubit gates with an error per gate of $3.8(1) \times 10^{-5}$. By creating a Bell state with a deterministic two-qubit gate, we deduce a gate error of $8(4) \times 10^{-4}$. We characterize the errors in our implementation and discuss methods to further reduce imperfections towards values that are compatible with fault-tolerant processing at realistic overhead.

DOI: 10.1103/PhysRevLett.117.060505

Quantum computers can solve certain problems that are thought to be intractable on conventional computers. An important general goal is to realize universal quantum information processing (QIP), which could be used for algorithms having a quantum advantage over processing with conventional bits as well as to simulate other quantum systems of interest [1–3]. For large problems, it is generally agreed that individual logic gate errors must be reduced below a certain threshold, often taken to be around 10^{-4} [4–6], to achieve fault tolerance without excessive overhead in the number of physical qubits required to implement a logical qubit. This level has been achieved in some experiments for all elementary operations including state preparation and readout, with the exception of two-qubit gates, emphasizing the importance of improving multiqubit gate fidelities.

Trapped ions are one candidate for scalable QIP. State initialization, readout, and quantum logic gates have been demonstrated in several systems with small numbers of trapped ions using various atomic species including $^9Be^+$, $^{25}Mg^+$, $^{40}Ca^+$, $^{43}Ca^+$, $^{88}Sr^+$, $^{111}Cd^+$, $^{137}Ba^+$, and $^{171}Yb^+$. The basic elements of scalable QIP have also been demonstrated in multizone trap arrays [7,8]. As various ions differ in mass, electronic, and hyperfine structure, they each have technical advantages and disadvantages. For example, $^9Be^+$ is the lightest ion currently considered for QIP, and as such, has several potential advantages. The relatively light mass yields a larger trap depth (inversely proportional to the mass) which can reduce ion loss from elastic collisions. Light mass also yields higher motional frequencies for given applied potentials, facilitates fast ion transport [9,10], and yields stronger laser-induced effective spin-spin coupling, which leads to a less spontaneous emission error for a given laser beam intensity [11]. However, a disadvantage of $^9Be^+$ ion qubits compared to some heavier ions such as $^{40}Ca^+$ and $^{43}Ca^+$ [12,13] has been the difficulty of producing and controlling the ultraviolet (313 nm) light required to drive $^9Be^+$ stimulated-Raman transitions. In the work reported here, we use an ion trap array designed for scalable QIP [14] and take advantage of recent technological developments with lasers and optical fibers that improve beam quality and pointing stability. We also implement active control of laser pulse intensities to reduce errors. We demonstrate laser-induced single-qubit computational gate errors of $3.8(1) \times 10^{-5}$ and realize a deterministic two-qubit gate to ideally produce the Bell state $|\Phi_+\rangle = (1/\sqrt{2})(|\uparrow\uparrow\rangle + |\downarrow\downarrow\rangle)$. By characterizing the effects of known error sources with numerical simulations and calibration measurements, we deduce an entangling gate infidelity or error of $\epsilon = 8(4) \times 10^{-4}$, where $\epsilon = 1 - F$, and F is the fidelity. Along with Ref. [13]; these appear to be the highest two-qubit gate fidelities reported to date.

The ions are confined in a multisegmented linear Paul trap (Fig. 1) designed to demonstrate scalable QIP [14–16]. Radio frequency (RF) potentials, with frequency $\omega_{RF} \simeq 2\pi \times 83$ MHz and amplitude $V_{RF} \simeq 200$ V, are applied to the RF electrodes to provide confinement transverse to the main trap channels. Control potentials are applied to the segmented control electrodes to create potential wells for the trapping of ions at desired locations in the channels. By applying time-dependent potentials to these electrodes, the ions can be transported deterministically between different trap zones. The trap also contains a junction at $\mathcal{C}$, which can be used for reordering [14]. For the experiment here, the ions are first loaded in $\mathcal{L}$ and then transported to $\mathcal{E}$. Quantum logic experiments described below are performed with ions confined in a fixed harmonic well at $\mathcal{E}$. Because of the particular design of the junction and trap imperfections, the ions undergo residual RF "micromotion" at frequency ω_{RF} along $\hat{z}$ with amplitude $\simeq$105 nm at $\mathcal{E}$. This affects our implementation of logic gates, Doppler and ground state cooling, and qubit state measurement, as described below.

For a single $^9Be^+$ ion confined in $\mathcal{E}$, the axial z harmonic mode frequency is $\omega_z \simeq 2\pi \times 3.58$ MHz, while the

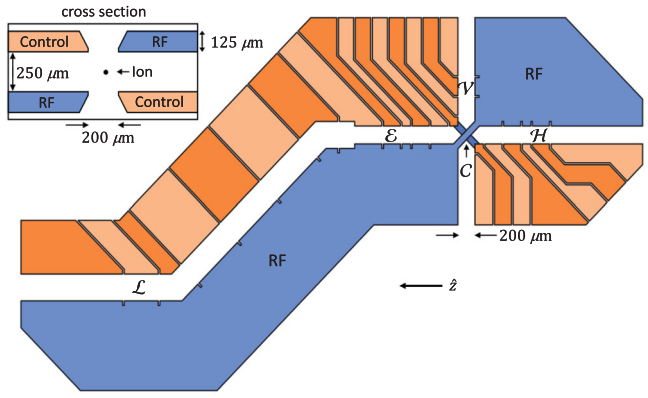

FIG. 1. Schematic of the ion trap, formed with two gold-coated, stacked wafers [14]. Top view of the trap (on the right) showing the load zone $\mathcal{L}$ and experiment zone $\mathcal{E}$. Ions are transported from $\mathcal{L}$ to $\mathcal{E}$ with time-varying potentials applied to the segmented control electrodes (colored orange hues). The positions of RF and control electrodes are exchanged in the lower layer (cross section in inset). Coherent manipulations are implemented on ions confined in $\mathcal{E}$.

transverse mode frequencies are $\omega_x \simeq 2\pi \times 11.2$ MHz, and $\omega_y \simeq 2\pi \times 12.5$ MHz. The ground state hyperfine levels and relevant optical levels for $^9Be^+$ ions in a magnetic field $B \simeq 0.0119$ T are shown schematically in Fig. 2. The qubit is encoded in the $^2S_{1/2}|F = 2, m_F = 0\rangle = |\downarrow\rangle$ and $|1, 1\rangle = |\uparrow\rangle$ hyperfine levels, where F and m_F are the total angular momentum and its projection along the quantization axis, respectively. The qubit frequency, $\omega_0 = 2\pi \times f_0 \simeq 2\pi \times 1207.496$ MHz is first-order insensitive to magnetic field fluctuations [17]; we measure a coherence time of approximately 1.5 s. Before each experiment, we Doppler cool and optically pump the ion(s) to the $|2, 2\rangle$ state with three laser beams that are σ^+-polarized relative to the B field and drive the $^2S_{1/2}|2, 2\rangle \rightarrow {}^2P_{3/2}|3, 3\rangle$ cycling transition as well as deplete the $|1, 1\rangle$ and $|2, 1\rangle$ states (Fig. 2 and Supplemental Material [18]). Both ions are then initialized to their $|\uparrow\rangle$ state by applying a composite π pulse on the $|2, 2\rangle \rightarrow |\uparrow\rangle$ transition. After gate operations and prior to qubit state detection, population in the $|\downarrow\rangle$ state is transferred or "shelved" to either the $|1, -1\rangle$ or $|1, 0\rangle$ state and the $|\uparrow\rangle$ state is transferred back to the $|2, 2\rangle$ state (Supplemental Material [18]). We then apply the Doppler-cooling beam and observe fluorescence. In the two-ion experiments, for a detection duration of 330 μs, we detect on average approximately 30 photons for each ion in the $|\uparrow\rangle$ state, and approximately 2 photons when both ions are in the $|\downarrow\rangle$ state. Coherent qubit manipulation is realized via two-photon stimulated-Raman transitions [15,35] (Supplemental Material [18]). The required laser beams (Fig. 3) are directed to the trap via optical fibers [36] and focused to beam waists of approximately 25 μm at the position of the ions.

High-fidelity single-qubit gates are driven with copropagating beams $\boldsymbol{k}_{2a}$ and $\boldsymbol{k}_{2b}$ detuned by Δ from the $^2S_{1/2} \leftrightarrow {}^2P_{1/2}$ transition frequency with their frequency difference set to ω_0. In this copropagating beam geometry, single-qubit gates are negligibly affected by ion motion. We employ the randomized benchmarking technique described in Ref. [37] to characterize gate performance. Each computational gate consists of a Pauli gate (π pulse) followed by a (non-Pauli) Clifford gate ($\pi/2$ pulse) around the x, y, and z axes of the Bloch sphere, and identity gates. The π pulses are performed with two sequential $\pi/2$ pulses about the same axis, each with duration $\simeq 2$ μs. Rotations about the z axis are accomplished by shifting the phase of the direct digital synthesizer that is keeping track of the qubit's phase; the identity gate is implemented with a 1 μs wait time. From the results of the randomized benchmarking (Fig. 4), we deduce an error per computational gate of $3.8(1) \times 10^{-5}$. For $\Delta \simeq -2\pi \times 730$ GHz used here, the spontaneous emission error [11] is estimated to be 2.5×10^{-5}. The remaining error is dominated by Rabi rate

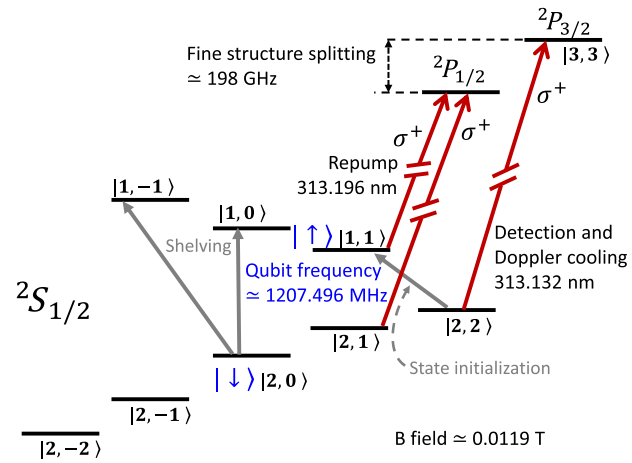

FIG. 2. Relevant energy level structure for $^9Be^+$ ions (not to scale). Transitions to the electronic excited states are used for Doppler cooling, repumping, and qubit state measurement as described in the text.

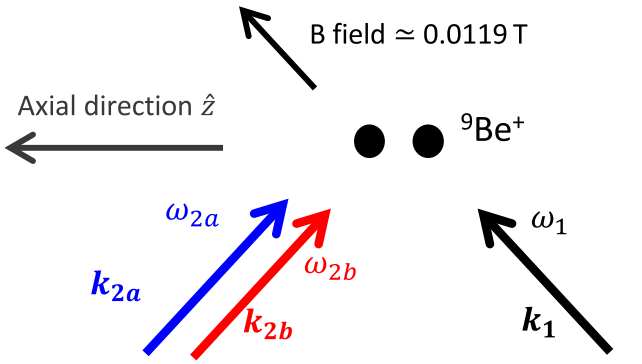

FIG. 3. Laser beam geometry for stimulated-Raman transitions. Copropagating beams $2a$ and $2b$ are used to implement high-fidelity single qubit gates; two-qubit entangling gates use all three beams as described in the text.

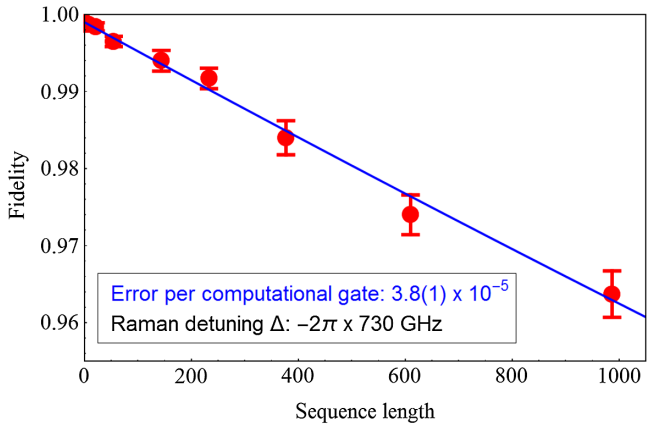

FIG. 4. Average fidelity for single-qubit-gate randomized benchmarking sequences, plotted as a function of sequence length. We determine the average error per computational gate to be $3.8(1) \times 10^{-5}$ and state preparation and measurement error to be $2.0(3) \times 10^{-3}$ for these data sets. Error bars show the standard error of the mean for each point.

fluctuations of approximately 1×10^{-3} due to imperfect laser power stabilization.

To couple the ions' internal ("spin") states to their motion, Raman transitions are driven by two beams along paths 1 and 2, respectively (Fig. 3). These beams intersect at 90° such that the difference in their $\boldsymbol{k}$ vectors, $\boldsymbol{\Delta k}$, is aligned along the axial direction, in which case only the axial motion will couple to the spins [15,35]. The strength of the spin-motion coupling provided by these beams is proportional to the single-ion Lamb-Dicke parameter $\eta = |\boldsymbol{\Delta k}| z_0 \simeq 0.25$ where $z_0 = \sqrt{\hbar/(2m\omega_z)}$, with $\hbar$ and m the reduced Planck's constant and the ion mass. However, due to the micromotion along the axial direction, the carrier and spin-motion sideband Rabi rates are reduced for this laser beam geometry. For our parameters, the modulation index due to the micromotion Doppler shift is approximately 2.9 such that the largest Rabi rates are provided by the second micromotion sideband which is reduced by a factor of $J_2(2.9) \simeq 0.48$ relative to Rabi rates in the absence of micromotion.

Two trapped ions confined in $\mathcal{E}$ align along the axial direction with spacing 3.94 μm. The relevant axial modes are the center-of-mass (C) mode (ions oscillate in phase at ω_z) and and "stretch" (S) mode (ions oscillate out of phase at $\sqrt{3}\omega_z$). The two-qubit entangling gate is implemented by applying an effective $\hat{\sigma}_x\hat{\sigma}_x$ type spin-spin interaction using state-dependent forces (here acting on the axial stretch mode) in a Mølmer-Sørensen (MS) protocol [38–41] using all three beams in Fig. 3 (Supplemental Material [18]). To maximize the spin-motion coupling and state-dependent forces with the ions undergoing micromotion, the three beam frequencies are set to $\omega_1 = \omega_L$, $\omega_{2a} = \omega_L + 2\omega_{\mathrm{RF}} - \omega_0 + \omega_S + \delta$, and $\omega_{2b} = \omega_L + 2\omega_{\mathrm{RF}} - \omega_0 - \omega_S - \delta$, where ω_L is the laser frequency, which is detuned by Δ from the $^2S_{1/2} \rightarrow {}^2P_{1/2}$ transition frequency, and δ is a small detuning ($\ll \omega_z$) that determines the gate duration [39]. Following initial Doppler cooling, the ions are sideband cooled with a series of $|2,2\rangle|n\rangle \rightarrow |\uparrow\rangle|n-1\rangle$ transitions, followed by repumping [35], resulting in mean mode occupation numbers $\langle n_C \rangle \simeq 0.01$ and $\langle n_S \rangle \simeq 0.006$ and the ions being pumped to the $|2,2\rangle$ state. Two-qubit measurements are made as in the one ion case, but we collect fluorescence from both ions simultaneously. We record photon count histograms with repeated experiments having the same parameters to extract the information about the qubit states.

We use the gate to ideally prepare the Bell state $|\Phi_+\rangle = (1/\sqrt{2})(|\uparrow\uparrow\rangle + |\downarrow\downarrow\rangle)$. To evaluate the gate's performance, we employ partial state tomography analyzed with a maximum likelihood (ML) algorithm to deduce the fidelity of the experimentally prepared state. Using a set of reference histograms, the maximum likelihood method estimates the experimentally created density matrix by maximizing the probability of the data histograms to correspond to that density matrix. The ML algorithm is general enough that joint-count histograms (here photon counts from two ions) can be analyzed without the need for individual addressing and measurement. From the Bell-state fidelity as determined by the ML method, we can estimate the MS gate fidelity. The ML Bell-state fidelity does not include errors due to imperfect $|2,2\rangle$ state

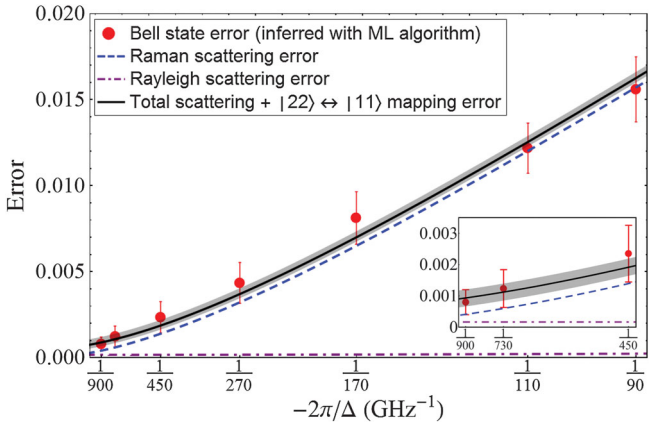

FIG. 5. ML Bell-state error (red dots), plotted as a function of $-2\pi/\Delta$ where Δ is the Raman detuning, for a constant gate duration of approximately 30 μs. The simulated contributions to the Bell state error from Raman and Rayleigh scattering (Supplemental Material [18]) are shown with the blue and purple dashed lines, respectively. For large $|\Delta|$ the Raman scattering error approaches zero, however, the Rayleigh scattering error remains approximately constant at 1.7×10^{-4}. The black line is the sum of the Raman and Rayleigh scattering errors and the error due to the composite microwave pulses used for qubit state preparation and detection (uncertainty indicated by the gray band). Error bars for the measured Bell state fidelity are determined from parametric bootstrap resampling [42] of the data and represent a 1σ statistical confidence interval.

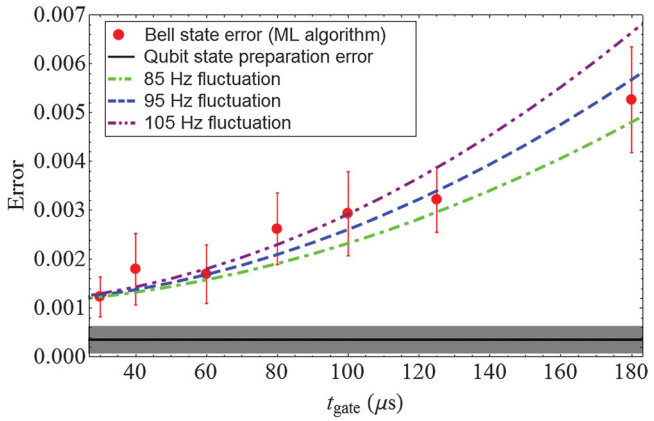

FIG. 6. ML Bell-state error (red dots) as a function of gate duration t_{gate} for a constant Raman beam detuning $\Delta \simeq -2\pi \times 730$ GHz. The black line shows the separately determined error and uncertainty (gray shade) due to the microwave pulses used for $|2,2\rangle \leftrightarrow |\uparrow\rangle$ state transfer. The three dashed lines show the sum of the expected gate errors including photon scattering and mode frequency fluctuations (which are slow compared to gate durations shown) for three different rms magnitudes of mode frequency fluctuations (Supplemental Material [18]). The gate error increases quadratically with increasing t_{gate} due to such frequency fluctuations; however, for $t_{gate} = 30$ μs the error due to these frequency fluctuations is approximately 1×10^{-4}.

preparation and measurement. By taking these effects into account we also determine a lower bound for the actual Bell-state fidelity (Supplemental Material [18]).

By varying the laser beam power, we determine the error of the Bell state as a function of Δ keeping a fixed gate duration of $\simeq 30$ μs (Fig. 5) and also as a function of gate duration for a fixed detuning $\Delta \simeq -2\pi \times 730$ GHz (Fig. 6). The various curves in the figures show the expected errors due to spontaneous emission and errors in the composite microwave pulses used for $|2,2\rangle \leftrightarrow |1,1\rangle = |\uparrow\rangle$ state transfer, and mode frequency fluctuations in Fig. 6. The minimum error obtained is $8(4) \times 10^{-4}$ for $\Delta \simeq -2\pi \times 900$ GHz and a gate duration of approximately 30 μs, which yields a ML Bell-state fidelity of 0.9992(4). An important contribution to the ML Bell-state error is due to the imperfect transfers from the $|2,2\rangle$ state to the qubit $|\uparrow\rangle$ state (for both qubits) before the application of the gate, and the reverse procedure that transfers $|\uparrow\rangle$ population back to the $|2,2\rangle$ state before detection. The total fidelity of these transfer pulses, limited by magnetic field fluctuations and the quality of the microwave pulses, is investigated with separate experiments analyzed with the same ML algorithm (Supplemental Material [18]), and we find $\epsilon_{transfer} = 4(3) \times 10^{-4}$. This is averaged over multiple data evaluations across multiple days; the uncertainty is the standard deviation of these data. While this error does not in principle affect the gate performance, we conservatively do not remove it from our gate fidelity estimate due to its relatively large uncertainty.

TABLE I. Individually determined errors for the entangling gate at a Raman detuning of $\Delta \simeq -2\pi \times 900$ GHz, and a gate duration of 30 μs. Off-resonant coupling includes coupling of the qubit states to other hyperfine states and their sidebands. The gate fidelity is determined from the Bell state analyzed with the ML method as described in the text.

Errors	$\times 10^{-4}$
Spontaneous emission (Raman)	4.0
Spontaneous emission (Rayleigh)	1.7
Motional mode frequency fluctuations	1
Rabi rate fluctuations	1
Laser coherence	0.2
Qubit coherence	< 0.1
Stretch-mode heating	0.3
Error from Lamb-Dicke approximation	0.2
Off-resonant coupling	< 0.1
$\|2,2\rangle \Leftrightarrow \|\uparrow\rangle$ two-way transfer	4

In the Supplemental Material [18], we describe in more detail characterization of individual errors sources through calibration measurements and numerical simulation. From this, we deduce that the fidelity of the ML Bell state is a good representation of the average gate fidelity. The errors for the highest state fidelity obtained are listed in Table I. It would be advantageous to evaluate the gate performance with full process tomography or randomized benchmarking to confirm our assessment. We did not perform randomized benchmarking because ion motional excitation gives additional errors. This excitation occurs during ion separation (to provide individual ion addressing) and because of anomalous heating [43] during the required long sequences of gates. These problems can eventually be solved as in Ref. [44] where the gate fidelity was measured by interleaved randomized benchmarking or by process tomography [45]. In both cases, the gate error was consistent with the measured two-qubit state fidelity. In the experiment here, the uncertainties of the inferred errors are deduced by parametric bootstrap resampling [42] with 500 resamples. We determine a lower bound of 0.999 on the purity of the $|2,2\rangle$ state for one ion prepared by optical pumping. With this, we put a lower bound of 0.997 on the overall Bell state fidelity.

In summary, we have demonstrated high fidelity single- and two-qubit laser-induced gates on trapped $^9Be^+$ ions. The single-qubit gate fidelity exceeds some threshold estimates for fault-tolerant error correction with reasonable overhead. Sources of the $\simeq 10^{-3}$ two-qubit gate error have been identified and can likely be reduced, making $^9Be^+$ ion a strong qubit candidate for fault-tolerant QIP. Gates with comparable fidelity have been recently reported by the Oxford group using $^{43}Ca^+$ ions [13].

This work was supported by the Office of the Director of National Intelligence (ODNI) Intelligence Advanced

Research Projects Activity (IARPA), ONR and the NIST Quantum Information Program. We thank D. Allcock and S. Brewer for helpful suggestions on the manuscript. We thank D. Hume, D. Lucas, C. Ballance, and T. Harty for helpful discussions. Contributions to this work by NIST, an agency of the U.S. Government, are not subject to U.S. copyright.

*tingrei.tan@nist.gov
†Present address: Physics Department and JILA, University of Colorado Boulder, Boulder, Colorado, USA.
‡Present address: Physics Department, University of Washington, Seattle, Washington, USA.

[1] R. P. Feynman, Int. J. Theor. Phys. **21**, 467 (1982).
[2] D. Deutsch, Proc. R. Soc. A **400**, 97 (1985).
[3] S. Lloyd, Science **273**, 1073 (1996).
[4] J. Preskill, Proc. R. Soc. A **454**, 385 (1998).
[5] E. Knill, Nature (London) **463**, 441 (2010).
[6] T. D. Ladd, F. Jelezko, R. Laflamme, Y. Nakamura, C. Monroe, and J. L. O'Brien, Nature (London) **464**, 45 (2010).
[7] J. P. Home, D. Hanneke, J. D. Jost, J. M. Amini, D. Leibfried, and D. J. Wineland, Science **325**, 1227 (2009).
[8] D. Hanneke, J. P. Home, J. D. Jost, J. M. Amini, D. Leibfried, and D. J. Wineland, Nat. Phys. **6**, 13 (2010).
[9] R. Bowler, J. Gaebler, Y. Lin, T. R. Tan, D. Hanneke, J. D. Jost, J. P. Home, D. Leibfried, and D. J. Wineland, Phys. Rev. Lett. **109**, 080502 (2012).
[10] A. Walther, F. Ziesel, T. Ruster, S. T. Dawkins, K. Ott, M. Hettrich, K. Singer, F. Schmidt-Kaler, and U. Poschinger, Phys. Rev. Lett. **109**, 080501 (2012).
[11] R. Ozeri, W. M. Itano, R. B. Blakestad, J. Britton, J. Chiaverini, J. D. Jost, C. Langer, D. Leibfried, R. Reichle, S. Seidelin, J. H. Wesenberg, and D. J. Wineland, Phys. Rev. A **75**, 042329 (2007).
[12] J. Benhelm, G. Kirchmair, C. F. Roos, and R. Blatt, Nat. Phys. **4**, 463 (2008).
[13] C. J. Ballance, T. P. Harty, N. M. Linke, and D. M. Lucas, arXiv:1406.5473; C. J. Ballance, T. P. Harty, N. M. Linke, M. A. Sepiol, and D. M. Lucas, preceding Letter, Phys. Rev. Lett. **117**, 060504 (2016).
[14] R. B. Blakestad, C. Ospelkaus, A. P. VanDevender, J. H. Wesenberg, M. J. Biercuk, D. Leibfried, and D. J. Wineland, Phys. Rev. A **84**, 032314 (2011).
[15] D. J. Wineland, C. Monroe, W. M. Itano, D. Leibfried, B. E. King, and D. M. Meekhof, J. Res. Natl. Inst. Stand. Technol. **103**, 259 (1998).
[16] D. Kielpinski, C. Monroe, and D. J. Wineland, Nature (London) **417**, 709 (2002).
[17] C. Langer, R. Ozeri, J. D. Jost, J. Chiaverini, B. DeMarco, A. Ben-Kish, R. B. Blakestad, J. Britton, D. B. Hume, W. M. Itano, D. Leibfried, R. Reichle, T. Rosenband, T. Schaetz, P. O. Schmidt, and D. J. Wineland, Phys. Rev. Lett. **95**, 060502 (2005).
[18] See Supplemental Material at http://link.aps.org/supplemental/10.1103/PhysRevLett.117.060505 for further details of experimental methods and data analysis, which includes Refs. [19–34].
[19] A. C. Wilson, C. Ospelkaus, A. P. VanDevender, J. A. Mlynek, K. R. Brown, D. Leibfried, and D. J. Wineland, Appl. Phys. B **105**, 741 (2011).
[20] D. R. Leibrandt and J. Heidecker, Rev. Sci. Instrum. **86**, 123115 (2015).
[21] R. Bowler, U. Warring, J. W. Britton, B. C. Sawyer, and J. M. Amini, Rev. Sci. Instrum. **84**, 033108 (2013).
[22] M. H. Levitt, Prog. NMR Spectrosc. **18**, 61 (1986).
[23] P. J. Lee, K.-A. Brickman, L. Deslauriers, P. C. Haljan, L.-M. Duan, and C. Monroe, J. Opt. B **7**, S371 (2005).
[24] T. R. Tan, J. P Gaebler, Y. Lin, Y. Wan, R. Bowler, D. Leibfried, and D. J. Wineland, Nature (London) **528**, 380 (2015).
[25] Z. Hradil, J. Řeháček, J. Fiurášek, and M. Ježek, *Quantum State Estimation* (Springer, New York, 2004), pp. 59–100.
[26] D. D. Boos, Stat. Sci. **18**, 168 (2003).
[27] Y. Lin, J. P. Gaebler, F. Reiter, T. R. Tan, R. Bowler, Y. Wan, A. Keith, E. Knill, S. Glancy, K. Coakley, A. S. Sørensen, D. Leibfried, and D. J. Wineland, arXiv:1603.03848.
[28] M. Horodecki, P. Horodecki, and R. Horodecki, Phys. Rev. A **60**, 1888 (1999).
[29] M. A. Nielsen, Phys. Lett. A **303**, 249 (2002).
[30] L. H. Pedersen, N. M. Møller, and K. Mølmer, Phys. Lett. A **367**, 47 (2007).
[31] D. Hayes, S. M. Clark, S. Debnath, D. Hucul, I. V. Inlek, K. W. Lee, Q. Quraishi, and C. Monroe, Phys. Rev. Lett. **109**, 020503 (2012).
[32] M. Harlander, M. Brownutt, W. Hänsel, and R. Blatt, New J. Phys. **12**, 093035 (2010).
[33] C. F. Roos, T. Monz, K. Kim, M. Riebe, H. Häffner, D. F. V. James, and R. Blatt, Phys. Rev. A **77**, 040302(R) (2008).
[34] X. R. Nie, C. F. Roos, and D. F. V. James, Phys. Lett. A **373**, 422 (2009).
[35] C. Monroe, D. M. Meekhof, B. E. King, S. R. Jefferts, W. M. Itano, D. J. Wineland, and P. Gould, Phys. Rev. Lett. **75**, 4011 (1995).
[36] Y. Colombe, D. H. Slichter, A. C. Wilson, D. Leibfried, and D. J. Wineland, Opt. Express **22**, 19783 (2014).
[37] K. R. Brown, A. C. Wilson, Y. Colombe, C. Ospelkaus, A. M. Meier, E. Knill, D. Leibfried, and D. J. Wineland, Phys. Rev. A **84**, 030303(R) (2011).
[38] A. Sørensen and K. Mølmer, Phys. Rev. Lett. **82**, 1971 (1999).
[39] A. Sørensen and K. Mølmer, Phys. Rev. A **62**, 022311 (2000).
[40] G. J. Milburn, S. Schneider, and D. F. V. James, Fortschr. Phys. **48**, 801 (2000).
[41] E. Solano, R. L. de Matos Filho, and N. Zagury, Phys. Rev. A **59**, R2539 (1999).
[42] B. Efron and R. J. Tibshirani, *An Introduction to the Bootstrap* (Chapman and Hall, London, 1993).
[43] Q. A. Turchette, D. Kielpinski, B. E. King, D. Leibfried, D. M. Meekhof, C. J. Myatt, M. A. Rowe, C. A. Sackett, C. S. Wood, W. M. Itano, C. Monroe, and D. J. Wineland, Phys. Rev. A **61**, 063418 (2000).
[44] J. P. Gaebler, A. M. Meier, T. R. Tan, R. Bowler, Y. Lin, D. Hanneke, J. D. Jost, J. P. Home, E. Knill, D. Leibfried, and D. J. Wineland, Phys. Rev. Lett. **108**, 260503 (2012).
[45] N. Navon, N. Akerman, S. Kotler, Y. Glickman, and R. Ozeri, Phys. Rev. A **90**, 010103(R) (2014).